Supplemental Material

Manuscript	GCM(s)/RCM(s)	AR detection criteria	AR change*	Precip change*
Shields and Kiehl 2016	High-resolution CCSM4	Wind and shape thresholds, as well as moisture anomalies that are based on relative anomalies similar to Zhu and Newell 1998 (i.e., will ignore changes due to more moisture)	Find changes (both increases and decreases) that are latitude/month dependent	Generally increased AR precipitation (looked at distributions during events)
Dettinger 2011	CMIP3 subset	IWV>2.5cm, upslope wind >10 m/s; only 1 grid point (central CA)	Modest increases in magnitude; nothing appreciable in frequency; DJF only	Did not examine
Hagos et al. 2016	CESM-LE	Bias-corrects model before analysis; PW>2cm+length+width requirement; 32-60N	Increase in AR frequency; DJF only	Decrease in the probability of extreme precipitation during AR days
Warner and Mass 2015	CMIP5 subset	IVT>99th historical percentile along near-coastal ocean grid points	Increases in future days exceeding historical 99th percentile	Increases in 99th percentile precipitation along same near-coastal ocean points
Radic et al. 2015	CMIP5 subset	SOM-based identification (trained on historical AR IVT)	Significant increase in all but one model; focused on British Columbia, Canada	Increase in total precipitation
Gao et al. 2015	CMIP5	Exceeding 85th percentile IVT, plus length and width criteria	Increase in the number of AR days for all coastal western US latitudes and seasons	Increases in AR-related precipitation
Lavers et al. 2015	CMIP5	None (not strictly examining ARs)	95th percentile IVT increases significantly in storm-track regions	Did not examine
Rivera and Dominguez 2016	NARCCAP and CMIP3 subset	IVT percentile-based (with varying percentiles for different locations)+length requirement	Increase in IVT but mixed frequency results across models (2 increase, 2 decrease)	Mixed results (both increases and decreases; inconsistencies across models)
Gershunov et al 2019	CMIP5, LOCA downscaled precipitation	IVT>250 kg/m/s, IWV>15mm, length>1500km, duration>18hours	Increase in AR frequency and intensity (more pronounced in their highest-quality GCMs)	Increase (Reduction) in CA wide AR (non-AR) precipitation

Table S1: Summary of selected recent manuscripts investigating response of ARs to climate change.

*end of century unless noted.

Model name (short name in parenthesis, where applicable)	
ACCESS1-0	GFDL-ESM2M* (GFDL)
ACCESS1-3	GISS-E2-H
BCC-CSM1-1-M	GISS-E2-R
BCC-CSM1-1	HADGEM2-AO
BNU-ESM	HADGEM2-CC
CAN-ESM2* (Can)	HADGEM2-ES* (HadGEM)
CCSM4	INMCM4
CESM1-BGC	IPSL-CM5A-LR
CESM1-CAM5	IPSL-CM5A-MR
CMCC-CESM	IPSL-CM5B-LR
CMCC-CM	MIROC-ESM-CHEM
CNRM-CM5	MIROC-ESM
CSIRO-MK3-6-0	MIROC5
EC-EARTH* (EC)	MPI-ESM-LR* (MPI)
FGOALS-G2	MPI-ESM-MR* (MPI)
FGOALS-S2	MRI-CGCM3
FIO-ESM	NORESM1-ME
GFDL-CM3	NORESM1-M
GFDL-ESM2G	

Table S2: CMIP5 simulations used in this manuscript. All simulations but EC-EARTH were used in the construction of Figure 1a. Simulations used as boundary conditions for NA-CORDEX are noted with an asterisk followed by parentheses containing the short naming convention used in Table 1.

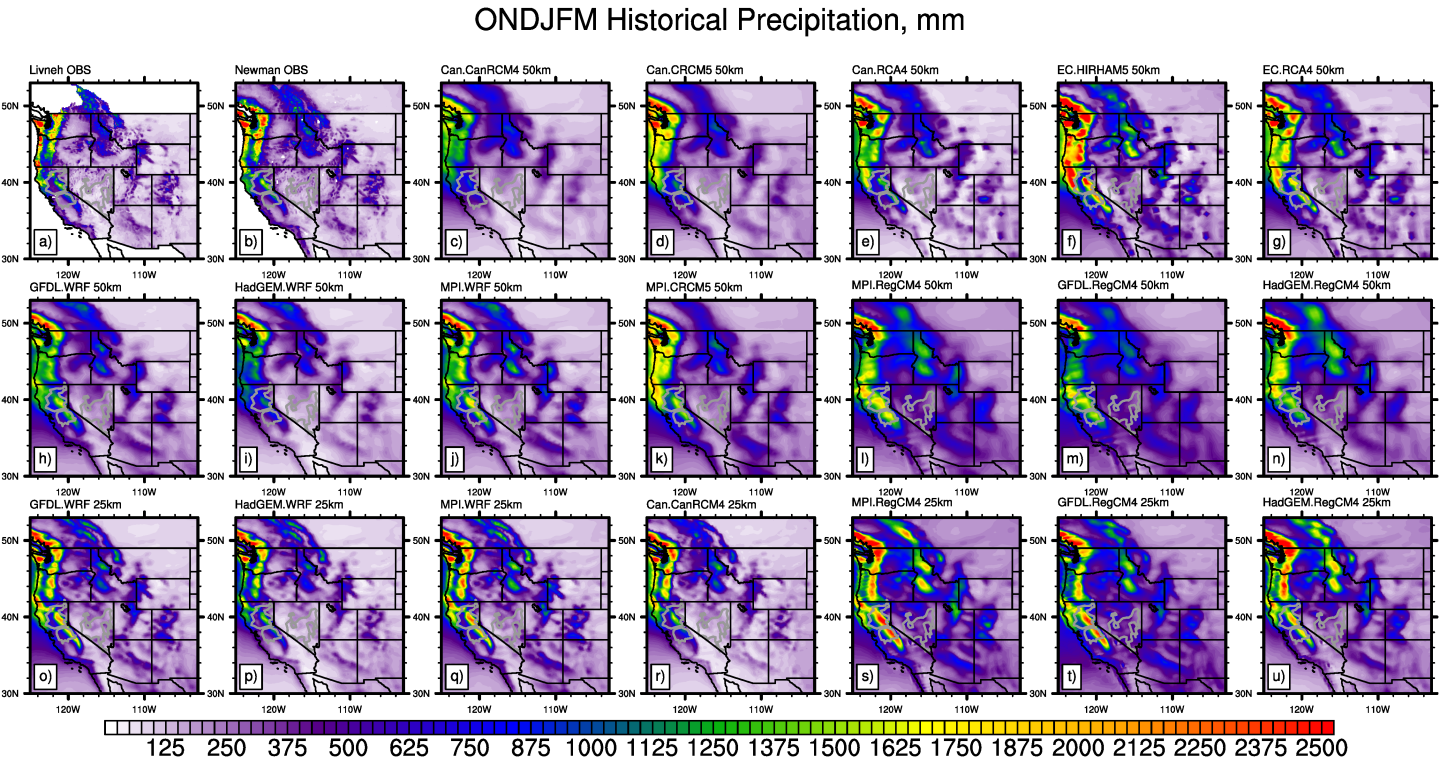

Figure S1: Cool season total mean precipitation (mm) (1979-2010) from (a) Livneh and (b) Newman observations-based datasets; (c-u) NA-CORDEX models. Gray contours outline three watersheds: Sacramento (top left), San Joaquin (bottom left), and Central Nevada River Basin (right).

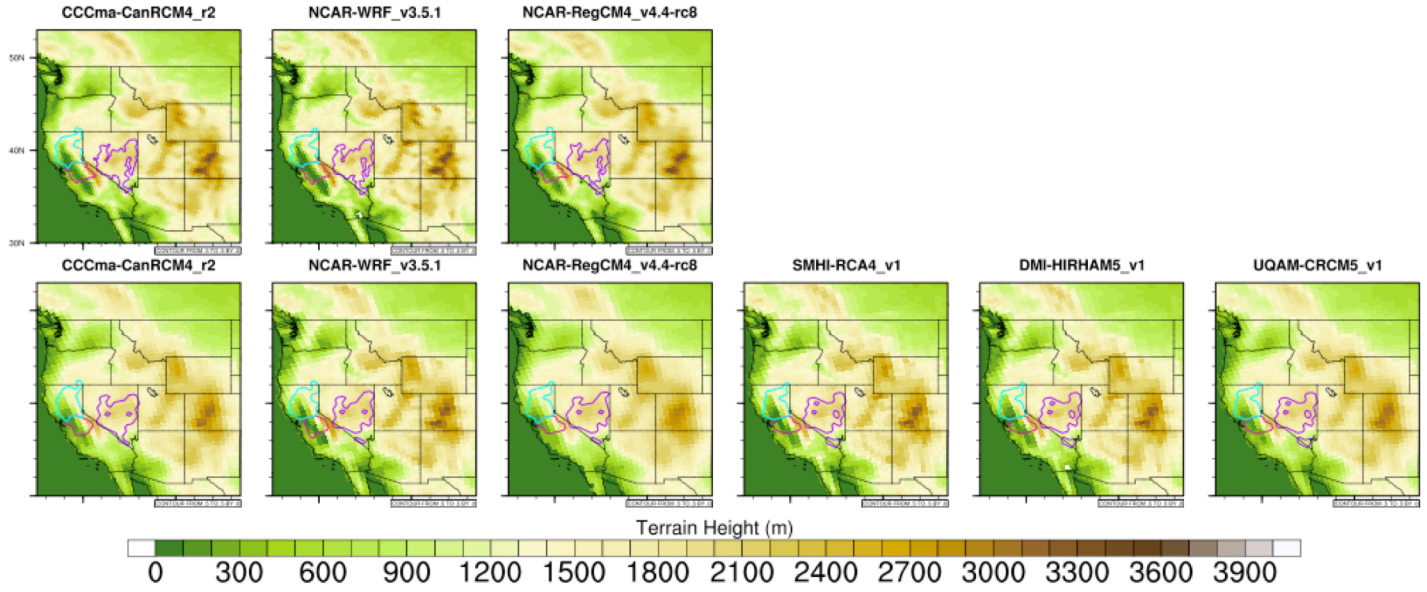

Figure S2: Terrain of each of the RCMs. Top row shows ~25 km RCMs and bottom row shows ~50 km RCMs. Cyan, red, and purple contours display locations of Sacramento, San Joaquin, and CNDB watersheds, respectively.

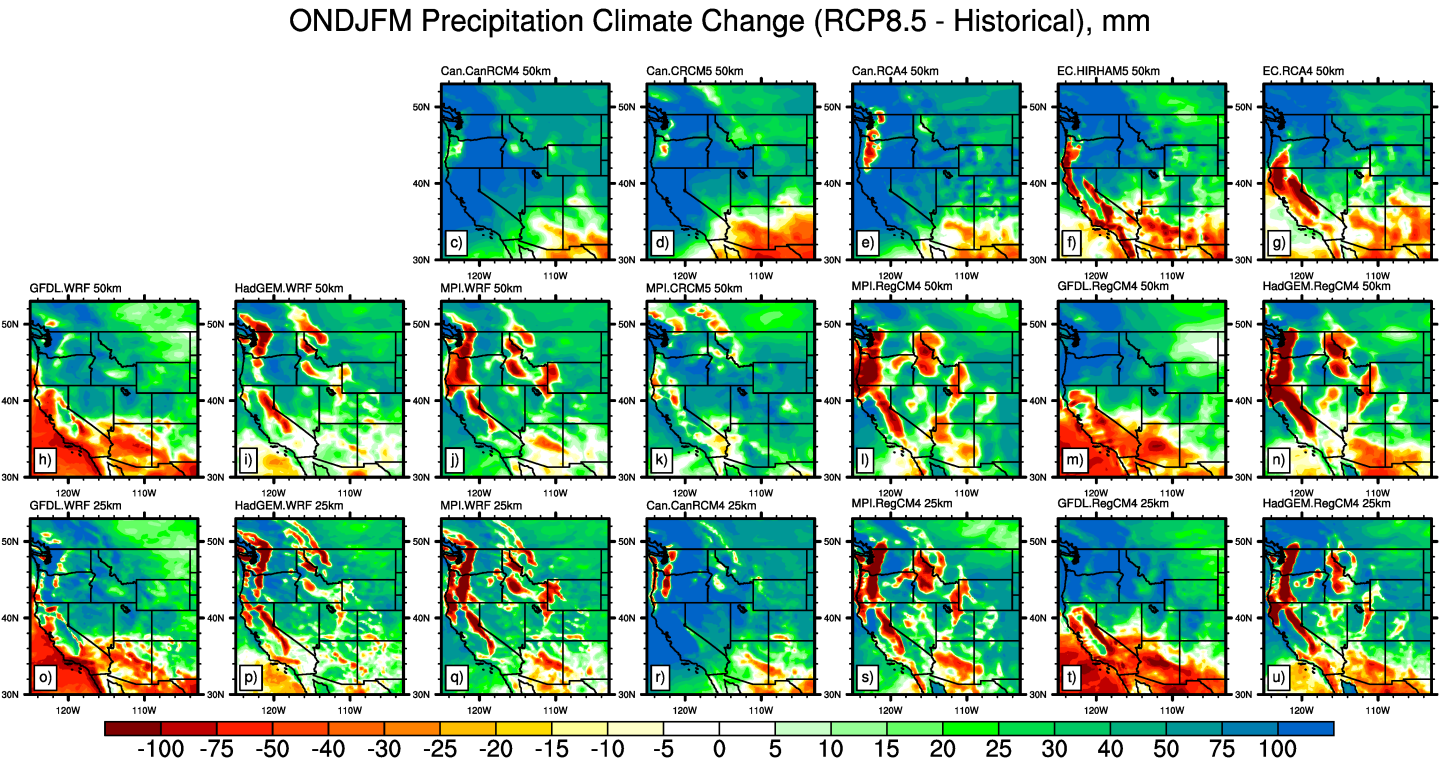

Figure S3: Cool season (ONDJFM) total mean precipitation change (mm) (RCP8.5 minus historical) from NA-CORDEX models. Note that (h-j) and (o-q) are identical to panels (d-f) and (g-i) of Figure 1, respectively, except for slightly differing color ranges.

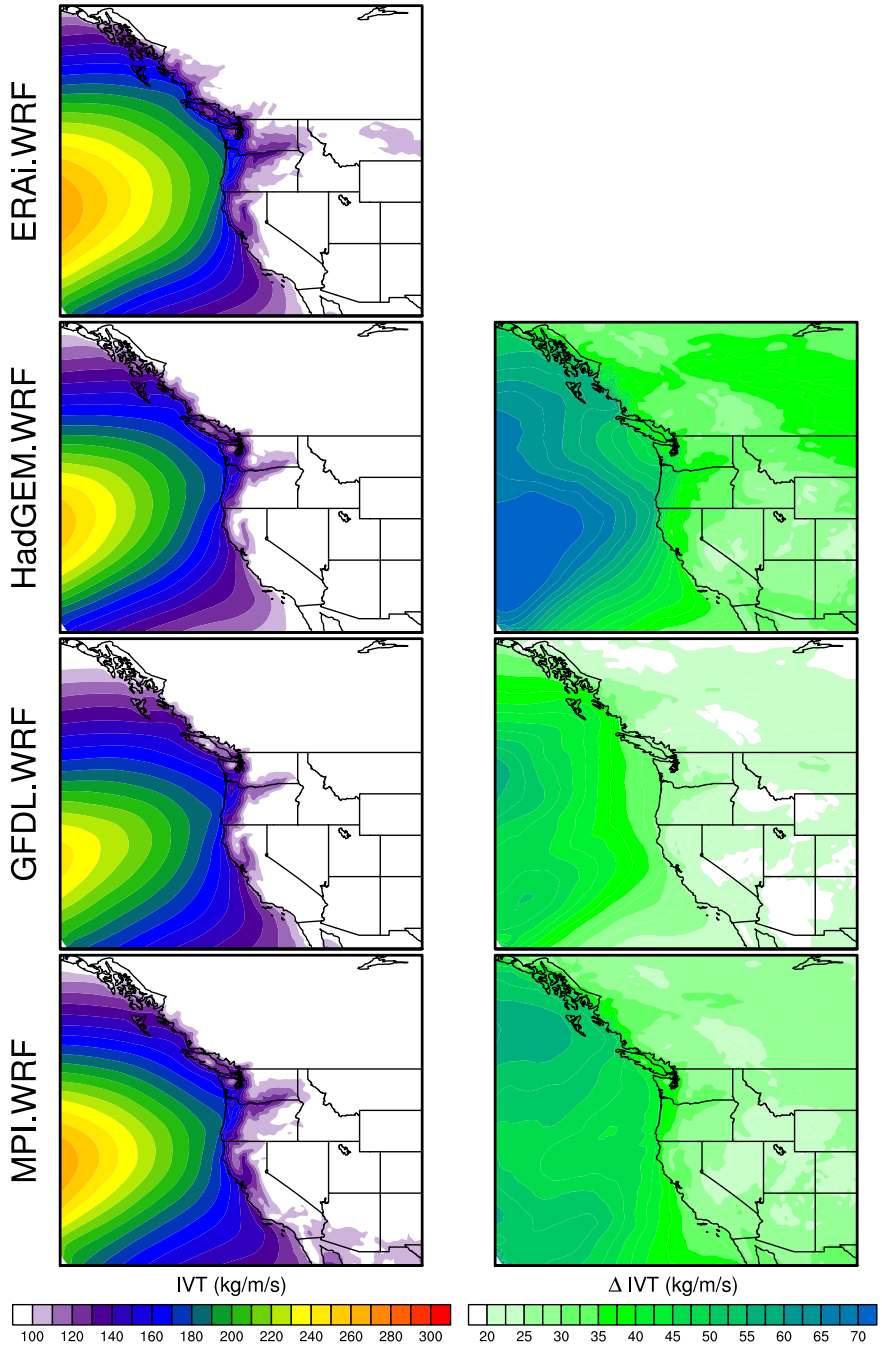

Figure S4: (left) Mean IVT during cool-season months (ONDJFM) during historical period (1980-2010), and (right) changes in cool-season IVT (future- historical), in 25 km WRF simulations.

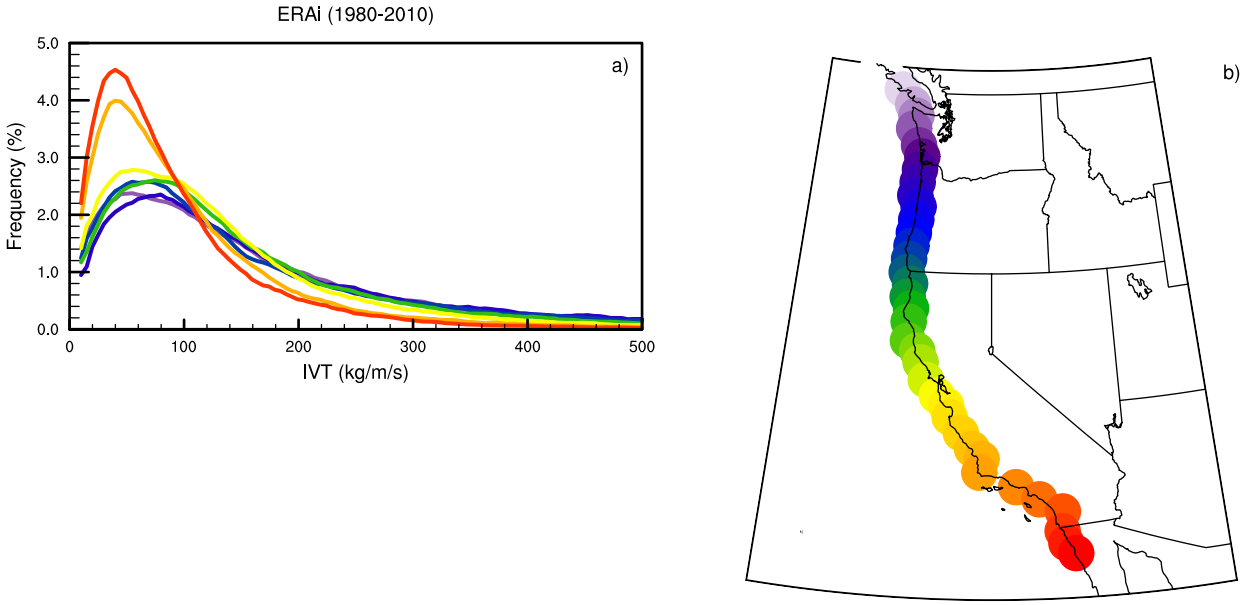

Figure S5: a) Estimated probability distribution functions of cool-season (ONDJFM) integrated water vapor transport (IVT) sampled every 3 hours at coastal locations (b) in the 1980-2010 25 km ERAi.WRF.

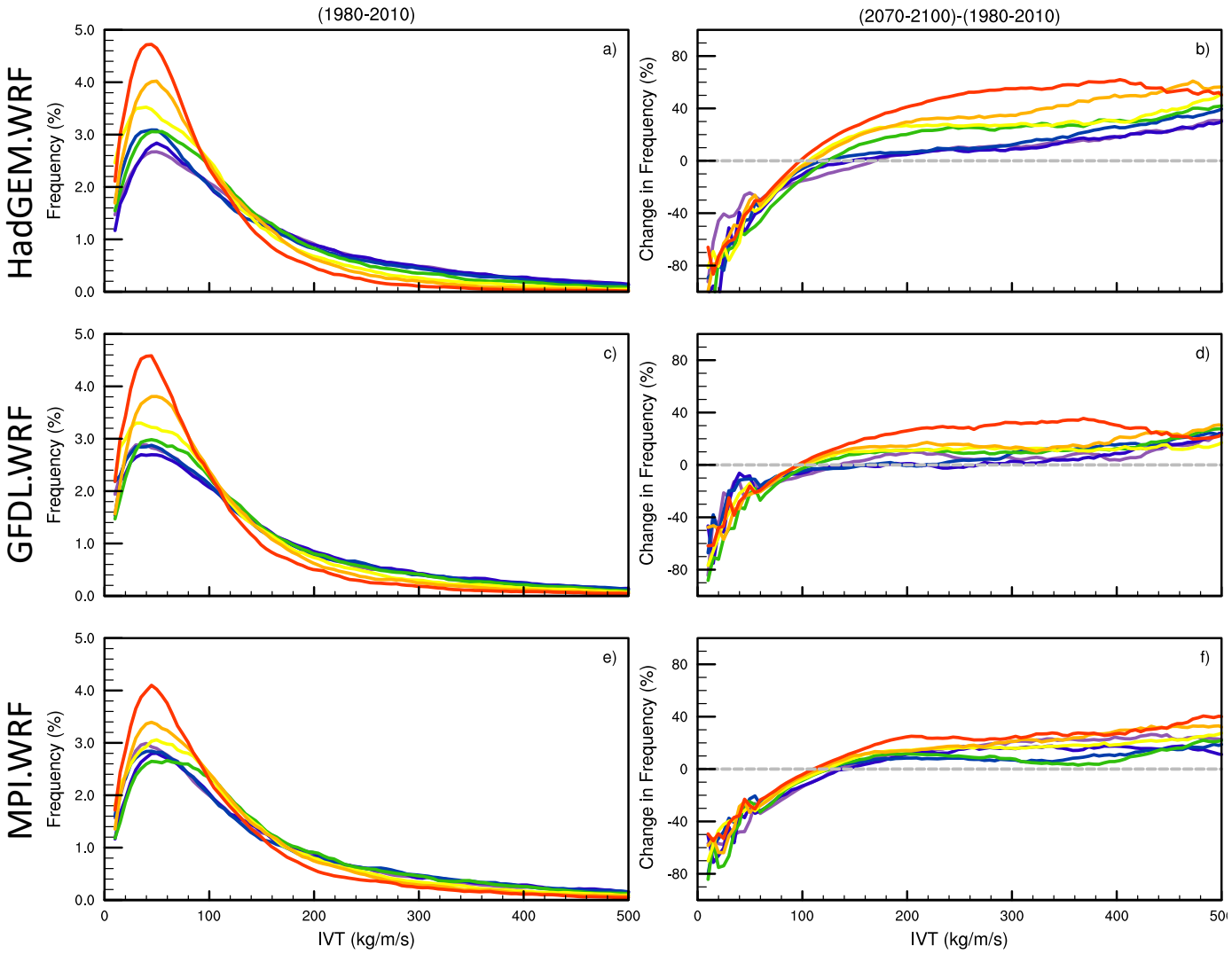

Figure S6: Estimated probability distribution functions (ePDF) of cool-season (ONDJFM) integrated water vapor transport (IVT) sampled every 3 hours at coastal locations (Figure S5b) during: (a, c, e) historical and (b, d, f) difference (i.e., future-historical) in IVT ePDF, for (a, b) 50 km HadGEM.WRF, (c, d) 50 km MPI-ESM-LR.WRF, (e, f) 50 km GFDL.WRF.

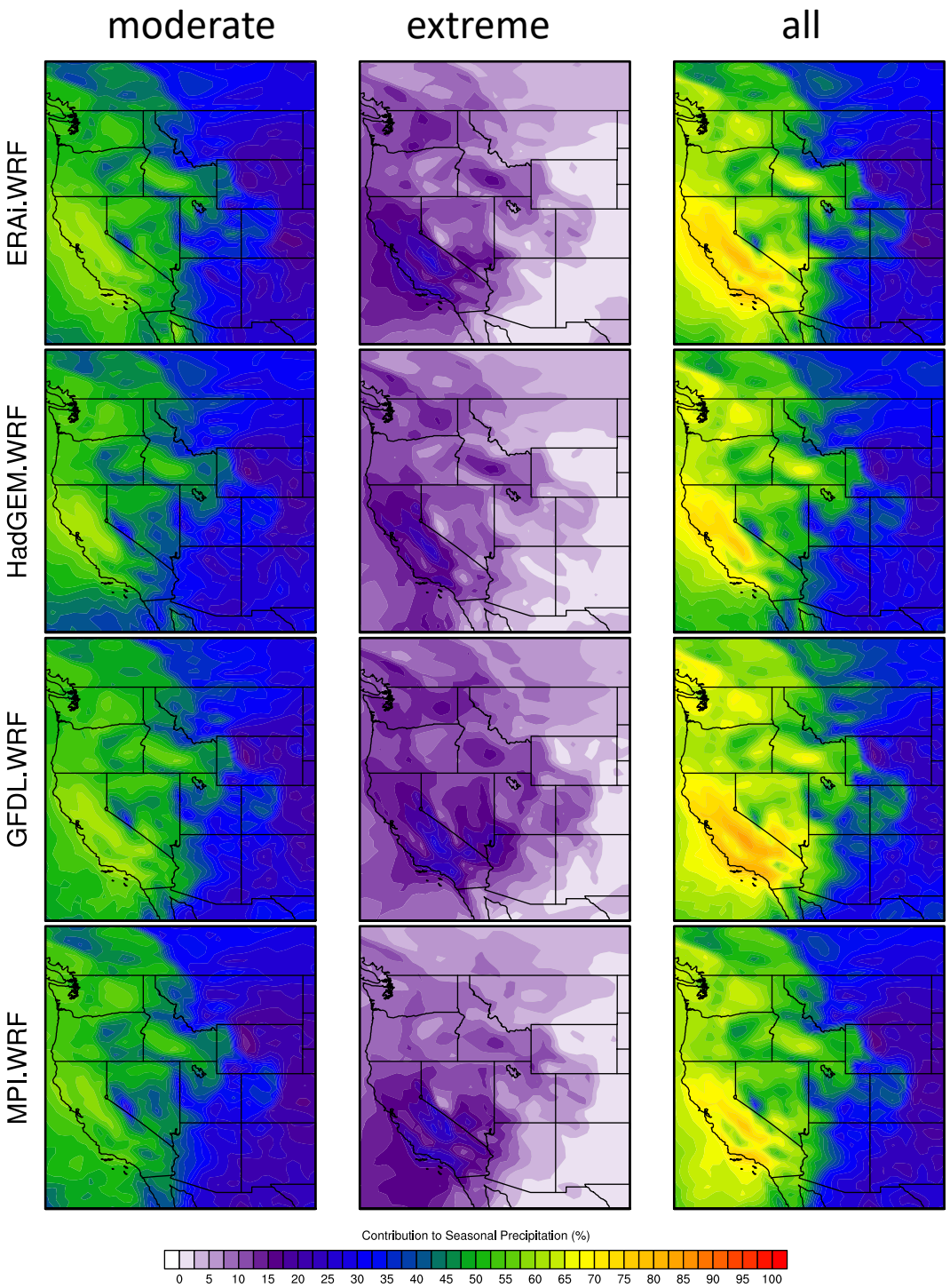

Figure S7: Contribution to cool season total precipitation associated with (left) moderate IVT events, (center) extreme IVT events, and (right) all IVT events in (top) ERAi.WRF, (second row) HadGEM.WRF, (third row) GFDL.WRF, and (bottom) MPI.WRF in 50 km WRF simulations.